Analysis of Postnatal Eye Development in the Mouse with High-Resolution Small Animal Magnetic Resonance Imaging

Tatiana V. Tkatchenko,[1] *Yimin Shen,*[2] *and Andrei V. Tkatchenko*[1,3]

Purpose. Studies of myopia in mice have been complicated by the difficulty in obtaining accurate measurements of small changes observed in the growing mouse eye in vivo and the lack of data on refractive eye development. The purpose of this study was to carry out an in vivo high-resolution analysis of mouse eye growth and refractive development.

Methods. High-resolution small animal magnetic resonance imaging and high-resolution infrared photorefraction were used to analyze refractive development in postnatal day (P)21 to P89 C57BL/6J mice.

Results. The growth of the mouse eye decelerated after P40. The eye maintained a slightly prolate shape during growth. The anterior chamber growth exhibited a similar pattern, whereas the corneal radius of curvature (CRC) increased linearly. The growth rate of the lens remained constant until P89. The lens "overgrew" the eye at P40, resulting in a decline in vitreous chamber depth. Mice showed myopic refractive errors at a younger age (−13.2 ± 2.0 D; mean ± SD, P21). The refractive errors stabilized around emmetropic values by P32 and remained emmetropic until P40. Mice became progressively hyperopic with age (+1.2 ± 1.7 D, P67; +3.6 ± 2.3 D, P89).

Conclusions. Development of ocular components in the mouse is similar to that of the tree shrew but different from that of higher primates and humans. Primary differences can be attributed to the age-related changes of the crystalline lens and CRC. In spite of these differences, mice appear to be able to achieve and maintain emmetropic refractive status at P32 to P40. (*Invest Ophthalmol Vis Sci.* 2010;51:21–27) DOI:10.1167/iovs.08-2767

Postnatal eye development is a tightly coordinated process whereby visual input regulates growth of the eye in a process called emmetropization.[1] Emmetropization is a result of the eye's capacity to adjust its growth during early postnatal development according to the quality of the image received by the retina. In the emmetropic primate eye, the refractive power of the optical media is tightly linked to the size of its vitreous chamber.[2,3] The failure of emmetropization often leads to the development of myopia. Approximately 20% to 30% of the myopic population has high myopia, which is often accompanied by serious complications such as retinal detachment and posterior staphyloma.[4] Myopia affects 33% of the adult population in the United States[5] and up to 80% of the school-age population in some parts of Asia,[6,7] and it represents the seventh leading cause of blindness.[4]

Degradation of the visual input by eyelid fusion, diffusers, or spectacle lenses during the early postnatal period has been shown to lead to the abnormal enlargement of the eye and the development of myopia in several vertebrate species, including nonhuman primates,[8] tree shrews,[9] and chickens.[10] The mouse, recently introduced as a model for myopia research, has a number of important advantages compared with other species traditionally used for studies of myopia. The mouse genome is completely sequenced and has 85% homology to the human genome.[11] This, combined with a number of well-established techniques for genome manipulation, has made it a very popular model for studies of visual system plasticity,[12–15] glaucoma,[16–18] retinal degeneration,[19–21] and behavioral studies of vision.[14,22–27] For the same reasons, the mouse may become a very powerful tool in studies of refractive eye development and myopia.

Several recent cross-sectional studies of postnatal mouse eye development have established the general pattern of postnatal mouse eye growth.[28–32] One study using optical low coherence interferometry (OLCI) measurements of the axial length suggested that the mouse eye stops growing at around postnatal day (P)40.[30] Nevertheless, other recent studies have suggested that the mouse eye grows in two phases,[28,29,31,32] that is, a period of rapid growth that lasts until P40 to P60 and a period of very slow eye expansion that continues up to P300. Several recent studies of refractive eye development in mice also produced mixed results.[30–32] Considering that all these studies were cross-sectional, their accuracy was reduced by the substantial individual variations within analyzed mouse populations. Thus, the postnatal growth pattern of the mouse eye and its refractive development have not yet been reliably characterized, primarily because of the small size of the mouse eye and substantial variations within mouse populations that masked small age-related changes in the dimensions of ocular components.

In the present study, we used high-resolution small animal magnetic resonance imaging (MRI) and high-resolution automated eccentric infrared photorefractometry to conduct a longitudinal study of the normal development of the refractive state and the dimensions of ocular components in C57BL/6J mice. We show that different eye components exhibit unique growth patterns during early postnatal development. We also show that, similar to other mammals, mice undergo emmetropization after birth. These results make the mouse a highly useful species for studies in refractive eye development and myopia.

From the Departments of [1]Anatomy and Cell Biology, [2]Radiology, and [3]Ophthalmology, Wayne State University, Detroit, Michigan.

Supported by National Eye Institute Grant 1R21EY018902 and Core Grant for Vision Research P30EY004068, Midwest Eye-Banks, and Research to Prevent Blindness.

Submitted for publication August 25, 2008; revised April 20, June 1 and 13, and July 11, 2009; accepted July 15, 2009.

Disclosure: **T.V. Tkatchenko**, None; **Y. Shen**, None; **A.V. Tkatchenko**, None

Corresponding author: Andrei V. Tkatchenko, Department of Anatomy and Cell Biology, Wayne State University, 540 E. Canfield Avenue, Detroit, MI 48201; atkatche@med.wayne.edu.

METHODS

Animals and Experimental Design

C57BL/6J mice were obtained from the Jackson Laboratory (Bar Harbor, ME) and were maintained as an in-house breeding colony at the Wayne State University School of Medicine. For the eye growth experiment, a group of C57BL/6J mice ($n = 4$) was analyzed using high-resolution small animal MRI. High-resolution MRI images of the right eye were collected at P21, P32, P40, P67, and P89. C57BL/6J mice are known to have a relatively high incidence of microphthalmia, which affects from 4.4% to 10% of animals.[33,34] Therefore, animals were screened for the presence of microphthalmia and other ophthalmic abnormalities, such as corneal opacities and anterior polar cataracts, often associated with this condition.[35] Animals found to have any deviation from the norm were removed from the study. All procedures adhered to the ARVO Statement for the Use of Animals in Ophthalmic and Vision Research and were approved by the Wayne State University Institutional Animal Care and Use Committee.

High-Resolution MRI

MRI was performed as previously described.[36] On the day of the examination, animals were anesthetized via intraperitoneal injection of ketamine (90 mg/kg) and xylazine (10 mg/kg). A contrast agent, gadopentetate dimeglumine (117 mg/mL, Magnevist; Berlex Laboratories, Wayne, NJ), was used as eyedrops to highlight the anterior chamber of the eye (see Supplementary Fig. S1, http://www.iovs.org/cgi/content/full/51/1/21/DC1, for an MRI image of the mouse eye without Magnevist [Berlex Laboratories]). Each mouse was then gently positioned on an MRI-compatible homemade holder. Animals were allowed to breathe spontaneously during the experiment. Rectal temperature was continuously monitored while the animal was inside the magnet. MRI data were acquired on a 4.7 T MRI system (Avance; Bruker BioSpin MRI GmbH, Ettlingen, Germany) using a two-turn transmit/receive surface coil (0.8-cm diameter) placed over the eye. The initial low-resolution scan in the horizontal plane of the eye was used to position the high-resolution scan in the sagittal plane of the eye. The plane for the high-resolution scan was positioned to go through the center of the lens, center of the cornea, and the optic nerve that ensured its proximity to the optical axis of the eye. Five serial low-resolution slices were collected using an adiabatic spin-echo imaging sequence (repetition time, 0.45 seconds; echo time, 13.6 ms; number of acquisitions, 1; matrix size, 256 × 128; slice thickness, 1 mm; field of view, 32 × 32 mm^2; 57 seconds for 5 slices). This resulted in an in-plane resolution of 125 μm^2. High-resolution images were collected using an adiabatic spin-echo imaging sequence (repetition time, 1 second; echo time, 13.6 ms; number of acquisitions, 4; matrix size, 512 × 512; slice thickness, 0.62 mm; field of view, 12 × 12 mm^2; 35 min/image). This resulted in an in-plane resolution of 23.4 μm^2. Sagittal virtual slices through the optical axis of the eye were obtained for each eye, and axial length, equatorial diameter, anterior chamber depth, anterior chamber width, lens thickness, vitreous chamber depth and circumference of the eye were measured using Scion Image (Scion, Frederick, MD) and derived macros. Five independent measurements were taken for each parameter and the mean ± SD were calculated.

Photorefraction

The refractive state of both left and right eyes was determined on alert animals using a high-resolution automated eccentric infrared photorefractor.[37] The animal to undergo refraction was immobilized using a restraining platform, and 1% tropicamide ophthalmic solution (Alcon Laboratories, Inc., Fort Worth, TX) was instilled in both eyes to ensure mydriasis and cycloplegia. Both eyes were refracted in the dark (<1 lux) after 5 to 7 minutes of tropicamide exposure along the optical axis. Five independent measurements (5–10 seconds long) were taken for each eye. Each measurement was marked by a green LED flash, which was registered by the photorefractor software. Sixty points (a point is acquired by the system every 16 ms) from each measurement immediately preceding the green LED flash were combined, and 300 points were used to calculate the mean ± SD.

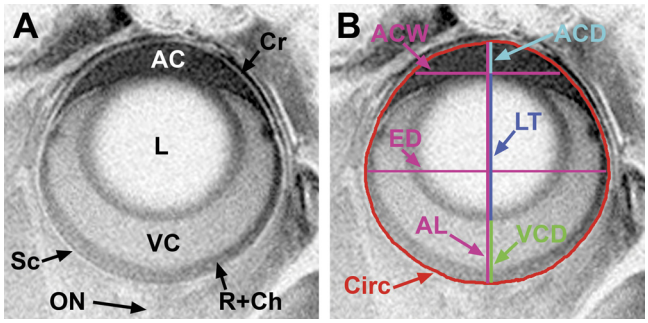

FIGURE 1. Typical magnetic resonance image of the mouse eye. (**A**) Various anatomic structures can be readily identified including cornea (Cr), anterior chamber (AC), lens (L), vitreous chamber (VC), retina plus choroid (R+Ch), sclera (Sc), and optic nerve (ON). (**B**) A variety of ocular parameters can be extracted from such images, including axial length (AL), equatorial diameter (ED), anterior chamber depth (ACD), anterior chamber width (ACW), vitreous chamber depth (VCD), lens thickness (LT), and circumference (Circ).

Statistical Analysis

Data modeling and analysis were performed using commercially available software packages (SigmaPlot; Systat Software, San Jose, CA, and STATISTICA; StatSoft, Tulsa, OK). Linear regression analysis and ANOVA were used to analyze correlations between refraction and changes in various ocular components with age. All data are presented as mean ± SD.

RESULTS

MRI of the Mouse Eye

To evaluate the feasibility of using small animal MRI to detect changes in eye dimensions in mice, we analyzed eye growth in C57BL/6J mice during the early postnatal period of development using a 4.7 T MRI system (Avance; Bruker). High-resolution sagittal slices of the right eye of each mouse through the optical axis were acquired as described in Methods (Fig. 1). Gadopentetate dimeglumine eyedrops provided clear outlines of the anterior chamber of the eye and substantially increased the accuracy of the anterior chamber measurements (Fig. 1A). A variety of ocular parameters can be extracted from such images, including axial length (AL), equatorial diameter (ED), anterior chamber depth (ACD), vitreous chamber depth (VCD), anterior chamber width (ACW), and lens thickness (LT) (Fig. 1B). AL was measured as the distance between the posterior surface of the cornea and the anterior surface of the sclera. ED was measured as the distance between the inner surfaces of the sclera. ACD was measured as the distance between the posterior surface of the cornea and the anterior pole of the lens. ACW was measured at the level of the anterior pole of the lens as the distance between the inner surfaces of the cornea. The ACD and ACW were used to calculate the corneal radius of curvature (CRC) as CRC = (ACD/2) + (ACW^2/(8 × ACD)). LT was determined as the distance between the anterior and posterior poles of the lens. VCD was measured between the posterior pole of the lens and the anterior surface of the sclera. Although xylazine was shown to reduce intraocular pressure in mice,[38] we had not encountered any problems in detecting differences in size (or absence of such differences) between the fellow eyes after ketamine/xylazine anesthesia because normal eye turgor was maintained.

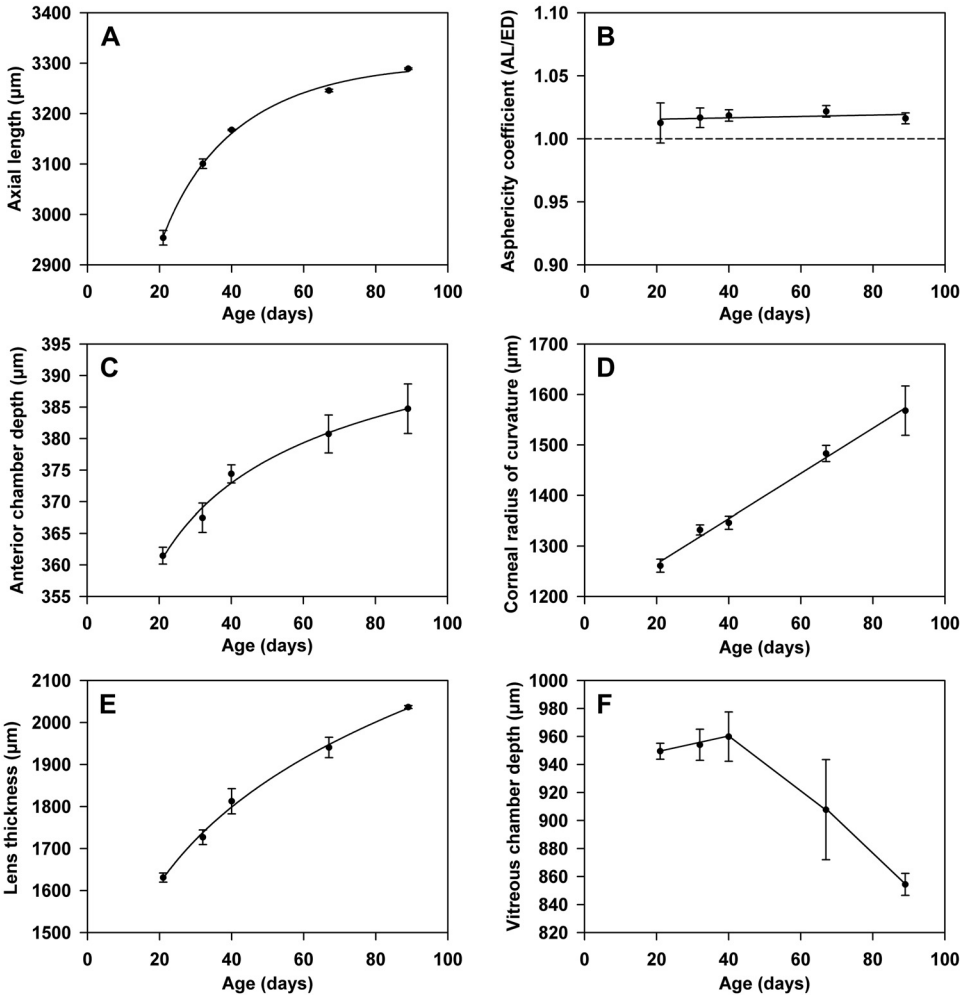

FIGURE 2. Development of the components of the mouse eye between 21 and 89 days of age. Various parameters were extracted from high-resolution magnetic resonance images of the right eye collected from a group of C57BL/6J mice at P21, P32, P40, P67, and P89. (**A**) AL. (**B**) Asphericity coefficient (R_a). R_a was calculated as a ratio between AL and ED. (**C**) ACD. (**D**) CRC. CRC was calculated as CRC = (ACD/2) + (ACW^2/(8 × ACD)). (**E**) LT. (**F**) VCD. n = 4. Vertical error bars, SD.

MRI Analysis of Postnatal Eye Growth in Mice

Sequential high-resolution images of the eye in a group of C57BL/6J mice were obtained at P21, P32, P40, P67, and P89 (Fig. 2, Table 1). Analysis of the axial length of the eye in this group of mice showed that the growth of the mouse eye decelerates with age, exhibiting three distinct phases during the first 89 days after birth (Fig. 2A, Table 1). Phase 1 (P21–P40) is characterized by a very rapid (11 μm/d, AL, $P = 0.002$) enlargement of the eyeball. The growth rate drops to 3 μm/d (AL, $P = 0.0005$) during the second phase (P40–P67) and slows to 2 μm/d (AL, $P = 0.0004$) during the third phase (P67–P89). The eye maintains a slightly prolate shape during these early stages of postnatal development (Fig. 2B, Table 1). A similar growth pattern was observed for the anterior chamber, which grows in size at a constant rate of 0.7 μm/d (ACD, $P = 0.16$) until P40, when its growth rate begins to level off (Fig. 2C, Table 1). The growth of the anterior chamber is accompanied by the linear increase in the CRC (P21–P89, 4.5 μm/d, $R = 0.997$, $P = 0.0002$; Fig. 2D, Table 1). The growth rate of the lens remains almost constant (6 μm/d, LT, $P = 0.0005$) until at least P89 (Fig. 2E, Table 1). The lens appears to overgrow the eye at about P40, resulting in a rapid decline (P40–P89, 2 μm/d, $P = 0.02$) of the VCD, which was increasing until this point at a rate of 0.6 μm/d (P21–P40, $P = 0.95$; Fig. 2F, Table 1).

Refractive Eye Development

We also analyzed age-related refractive eye development in the same group of C57BL/6J mice. The refractive errors were measured in both eyes at P21, P32, P40, P67, and P89 using the

TABLE 1. Age-Related Changes of Refraction and Ocular Component Dimensions in C57BL/6J Mice

Age (days)	Refraction (D)	AL (μm)	ED (μm)	ACD (μm)	CRC (μm)	LT (μm)	VCD (μm)
21	−13.2 ± 2.0	2954 ± 14	2932 ± 54	361 ± 1	1261 ± 13	1631 ± 11	949 ± 6
32	−0.5 ± 1.5	3100 ± 9	3050 ± 32	367 ± 2	1332 ± 10	1727 ± 17	954 ± 11
40	+0.3 ± 0.9	3168 ± 1	3110 ± 15	374 ± 1	1346 ± 13	1812 ± 30	960 ± 18
67	+1.2 ± 1.7	3246 ± 3	3177 ± 12	381 ± 3	1483 ± 16	1940 ± 24	908 ± 36
89	+3.6 ± 2.3	3289 ± 2	3236 ± 14	385 ± 4	1568 ± 49	2037 ± 4	854 ± 8

Data are shown as mean ± SD. D, diopters; AL, axial length; ED, equatorial diameter; ACD, anterior chamber depth; CRC, corneal radius of curvature; LT, lens thickness; VCD, vitreous chamber depth.

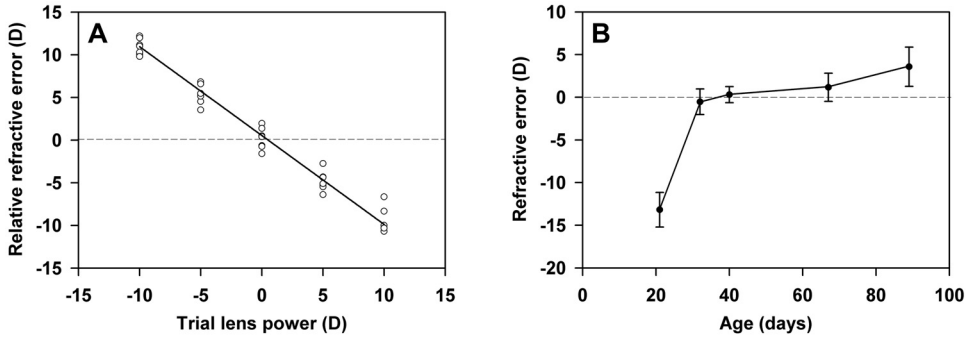

FIGURE 3. Refractive development of the mouse eye between 21 and 89 days of age. (**A**) Calibration of the high-resolution automated eccentric infrared photorefractor to the mouse eye (P40). Trial lenses of different power (−10, −5, 0, +5, and +10) were placed in front of the mouse eye, and measured refractive errors were recorded. (**B**) Age-related changes in refraction. Refractive errors stabilize around emmetropic values at P32 and remain emmetropic until P40. $n = 8$. Vertical error bars, SD.

automated eccentric infrared photorefractor (Fig. 3, Table 1). We found that young (P21) animals were highly myopic. The refractive errors were −13.2 ± 2.0 D at day 21 ($P < 0.0001$). However, this initial myopic refraction was followed by emmetropization. We found that the refractive state of the mouse eye stabilized around emmetropia at P32 (−0.5 ± 1.5 D; $P < 0.0001$) and remained in emmetropic range until P40 (+0.3 ± 0.9 D; $P < 0.0001$). Beginning with this age, we observed a hyperopic shift in refraction because P67 animals exhibited slight hyperopia (+1.2 ± 1.7 D; $P = 0.07$). The hyperopic shift in refraction increased with age. The average refractive error at day 89 reached +3.6 ± 2.3 D ($P < 0.0001$).

Correlation between Ocular Growth and Refractive Eye Development

Although we did not find a significant correlation between changes in ocular parameters and refraction in younger animals (P21–P32), we found a statistically significant correlation between the refractive error and various ocular parameters in

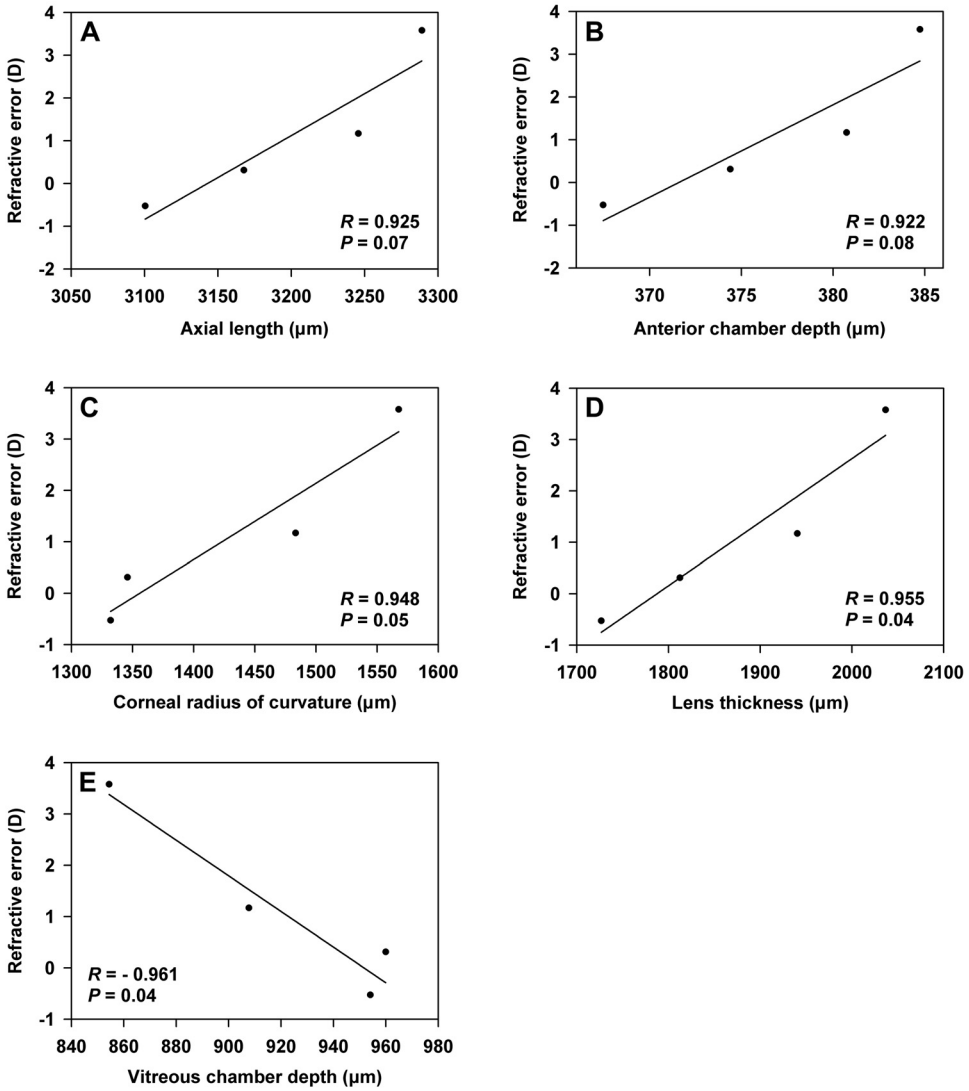

FIGURE 4. Correlation analysis between refraction and various ocular components in the mouse after P32. Linear regression analysis was performed to identify statistically significant age-related correlations. (**A**) Refractive error versus AL. (**B**) Refractive error versus ACD. (**C**) Refractive error versus CRC. (**D**) Refractive error versus LT. (**E**) Refractive error versus VCD. Data for P32, P40, P67, and P89 mice were used (Fig. 2, Table 1). Statistically significant correlations were identified between the refractive error and CRC, LT, and VCD.

older animals (P32–P89; Fig. 4). The refractive error positively correlated with CRC ($R = 0.948$, $P = 0.05$; Fig. 4C) and LT ($R = 0.955$, $P = 0.04$; Fig. 4D) and negatively correlated with VCD ($R = -0.961$, $P = 0.04$; Fig. 4E). We did not find a statistically significant correlation with either AL ($R = 0.925$, $P = 0.07$; Fig. 4A) or ACD ($R = 0.922$, $P = 0.08$; Fig. 4B).

Discussion

In cold-blooded vertebrates, such as amphibians and teleost fishes, all structural components of the eye continue to grow throughout life.[39–42] In warm-blooded vertebrates, including humans, the postnatal eye growth takes place during the early postnatal period of development.[43–47]

Postnatal Development of Ocular Components in the Mouse

The axial growth of the mouse eye appears to be similar to that of other warm-blooded vertebrate species. A recent study using OLCI measurements of axial length in a group of 23 animals suggested that the mouse eye stops growing at around P40.[30] This observation is supported by two reports that the refractive state of the juvenile mouse eye stabilizes at around P40.[31,48] However, three recent studies using measurements of eye weight,[29] measurements on frozen sections,[31] and OLCI[28] suggested that the mouse eye grows in two phases, a period of rapid growth, which lasts from eye opening at P14 through P40 to P60 (i.e., up to the age of sexual maturity), and a period of a very slow eye expansion, which continues up to P300. Our MRI data suggest that the mouse eye grows in three distinct phases during the first 3 months of postnatal development. The first phase, which is characterized by very rapid growth (11 μm/d, AL), lasts until P40. It is followed by a second phase, when the eye continues to grow at a reduced rate (3 μm/d, AL) until P67. The eye continues to grow even after this point, albeit at a very slow pace of approximately 2 μm/d, until P89 (the oldest animals we have analyzed). Despite the substantial deceleration of eye growth in P89 mice, the mouse eye appears to continue its growth beyond this point, in agreement with previous cross-sectional studies.[28,29,31,32] Similar age-related changes in AL have been reported in other mammalian species,[49–51] including humans.[46,52–56] We found that the depth of the anterior chamber continues to increase until P40 at a constant rate. After this point, it begins to level off as overall eye growth also begins to decelerate. Although our mouse anterior chamber data are similar to the data previously reported by others[28,31,32] and to the data of other mammals,[49,50,53–55,57–62] our data suggest that the anterior chamber displays linear growth longer than previously demonstrated. Contrary to the recent cross-sectional study by Zhou et al.,[32] we found that CRC exhibits a linear increase until P89. This is similar to what is observed in other mammalian species in which CRC exhibits an increase during the early postnatal period of development[46,49,50,53–56,58–62]; however, CRC increases at higher rate than in primates. The mouse crystalline lens continues to grow at a constant rate until P89 (the oldest animals we have analyzed) and obviously overgrows the rest of the eye at P40, as the depth of the vitreous chamber begins to decline after that age. This result is different from what was recently reported by Zhou et al.[32] but is similar to age-related changes in the crystalline lens and VCD observed in the tree shrew.[49] The age-related lens and VCD changes observed in the mouse and the tree shrew during the early postnatal period are different from what is described in higher primates and humans.[46,50,53–56,62–68] In *Macaca mulatta*, the initial increase in the lens thickness that continues until 12 months of age (corresponds to P40 in mice) is followed by lens thinning at 12 to 27 months of age (corresponds to P40–P89 in mice), whereas VCD increases throughout the early postnatal period.[50] In *Homo sapiens*, initial lens thinning at 3 to 10 years of age (corresponds to P21–P67 in mice) is followed by the steady increase in the lens thickness that continues throughout life.[53,54,56,64–70] VCD increases in humans throughout the early postnatal period, similar to what has been observed in *M. mulatta*.[53–55,62,63] Thus, our data suggest that the axial growth of the mouse eye is similar to the axial eye growth in primates and humans.[46,49,50,52–55,71] The main differences between mice and higher primates and humans lie with the lens and the vitreous chamber. Although lens thickening causes a decrease in VCD in older monkeys and in humans older than 20 years,[51,69] it takes place later in postnatal development than in mice. Interestingly, the wet weight of the human crystalline lens exhibits a linear growth during postnatal development similar to what we have observed in mice.[72] However, the mouse lens is rounder, less plastic, and occupies a larger portion of the eye than the human lens.[73] Mice also lack accommodation because of the rigidity of the lens and the absence of the ciliary muscle.[73,74] Therefore, the mouse lens does not undergo flattening caused by lateral stretching exerted by the growing eye during the early postnatal period, whereas the human lens does. The growth rate of the mouse lens is also higher than it is in higher primates and humans. Thus, physiological differences between the mouse lens and the lens of higher primates and humans may explain the differences between mice and higher primates and humans in age-related changes of the lens and VCD during the early postnatal period. Lens thickening and the decline in VCD occur in higher primates and humans later in development.

Postnatal Refractive Development in the Mouse

Several studies of the normal refractive development in the mouse have suggested that mice, unlike other mammalian species, are born hyperopic and become even more hyperopic with age.[31,37,75,76] Although a recent study by Zhou et al.[32] reported myopic refractive errors in younger animals (P22–P25), it also suggested that the refractive state of the mouse eye stabilizes at highly hyperopic values with age. Although these studies differed from each other with regard to the exact refraction values associated with particular ages, they all suggested that mice do not undergo emmetropization similar to other mammalian species. Contrary to these reports, we found that C57BL/6J mice are born highly myopic (-13.2 ± 2.0 D, P21) and then undergo emmetropization during the first month after birth. The refractive errors stabilize around emmetropic values at P32 and remain emmetropic until P40. Beginning at that age, C57BL/6J mice become progressively hyperopic ($+1.2 \pm 1.7$ D, P67; $+3.6 \pm 2.3$ D, P89). This is consistent with our MRI data suggesting that the mouse eye should become progressively hyperopic after P40 because the increasing CRC and decreasing VCD would result in a hyperopic shift in refraction. This conclusion is also supported by correlation data indicating that the refractive state of the mouse eye after P32 is determined by the changes in the CRC and vitreous chamber. The correlation between refraction and LT may be secondary and simply a reflection of the role the lens plays in setting the limits of the vitreous chamber.

The highly hyperopic refractive errors previously reported in adult mice are likely to represent an artifact of measurement. Several different approaches have been used to measure refractive errors in mice, such as streak retinoscopy on the animals anesthetized with ketamine/xylazine,[75] photorefraction of the animals anesthetized with ketamine/xylazine,[76] and photorefraction of freely moving alert mice using the high-resolution automated eccentric infrared photorefractor.[31,32,37] We also

used an automated infrared photorefractor, but our approach was different in that we subjected to refraction alert animals that were immobilized using a restraining platform to ensure refraction along the optical axis. The highly hyperopic refractive errors found in mice with streak retinoscopy were attributed to the "small eye artifact" that was suggested to result from the reflection of retinoscope light from the boundary between vitreous and retina.[77] However, further detailed studies of the optical properties of ocular tissues did not support the small eye artifact hypothesis and concluded that light is primarily reflected by the retinal pigment epithelium (RPE).[78–83] Considering that the reflective properties of the fundus at the level of the RPE are even more pronounced in infrared light,[78,79] the hyperopic refractive errors recorded with infrared photorefractometry cannot be explained by the small eye artifact. Therefore, we have analyzed the effect of ketamine/xylazine anesthesia on refraction in mice and found that ketamine/xylazine alone causes a hyperopic shift in refraction of 6.8 ± 2.4 D ($P < 0.0001$). We also compared refraction data with and without the use of a restraining platform and noticed a persistent hyperopic shift when animals underwent refraction without restraint. This can be explained by the fact that refraction of freely moving mice along the optical axis of the eye is virtually impossible. Because the mouse eye has a prolate shape (Fig. 2B) and, therefore, is increasingly hyperopic off optical axis, refractive measurements obtained from moving animals will have hyperopic values.

Thus, our data suggest that the development of ocular components in the mouse is similar to that in the tree shrew but somewhat different from that in higher primates and humans. The primary differences can be attributed to the age-related changes of the crystalline lens during the early postnatal period. In spite of these differences, mice can achieve and maintain a relatively emmetropic refractive status at P32 to P40.

Acknowledgments

The authors thank the staff of the Wayne State University MR Research Facility for assistance with small animal MRI, Robert N. Frank for help with the manuscript, and Elio Raviola and William K. Stell for helpful discussions.

References

1. Curtin BJ. *The Myopias: Basic Science and Clinical Management.* Philadelphia: Harper & Row; 1985.
2. Smith EL 3rd, Hung LF. The role of optical defocus in regulating refractive development in infant monkeys. *Vision Res.* 1999;39:1415–1435.
3. Zhong X, Ge J, Nie H, Chen X, Huang J, Liu N. Effects of photorefractive keratectomy-induced defocus on emmetropization of infant rhesus monkeys. *Invest Ophthalmol Vis Sci.* 2004;45:3806–3811.
4. Alexander LJ. *Primary Care of the Posterior Segment.* 2nd ed. East Norwalk, CT: Appleton & Lange; 1994.
5. Vitale S, Ellwein L, Cotch MF, Ferris FL 3rd, Sperduto R. Prevalence of refractive error in the United States: 1999–2004. *Arch Ophthalmol.* 2008;126:1111–1119.
6. Lam CS, Goldschmidt E, Edwards MH. Prevalence of myopia in local and international schools in Hong Kong. *Optom Vis Sci.* 2004;81:317–322.
7. Lin LL, Shih YF, Hsiao CK, Chen CJ. Prevalence of myopia in Taiwanese schoolchildren: 1983 to 2000. *Ann Acad Med Singapore.* 2004;33:27–33.
8. Wiesel TN, Raviola E. Myopia and eye enlargement after neonatal lid fusion in monkeys. *Nature.* 1977;266:66–68.
9. Sherman SM, Norton TT, Casagrande VA. Myopia in the lid-sutured tree shrew (*Tupaia glis*). *Brain Res.* 1977;124:154–157.
10. Wallman J, Turkel J, Trachtman J. Extreme myopia produced by modest change in early visual experience. *Science.* 1978;201:1249–1251.
11. Waterston RH, Lindblad-Toh K, Birney E, et al. Initial sequencing and comparative analysis of the mouse genome. *Nature.* 2002;420:520–562.
12. Gordon JA, Stryker MP. Experience-dependent plasticity of binocular responses in the primary visual cortex of the mouse. *J Neurosci.* 1996;16:3274–3286.
13. Huang ZJ, Kirkwood A, Pizzorusso T, et al. BDNF regulates the maturation of inhibition and the critical period of plasticity in mouse visual cortex. *Cell.* 1999;98:739–755.
14. Prusky GT, Douglas RM. Developmental plasticity of mouse visual acuity. *Eur J Neurosci.* 2003;17:167–173.
15. Tagawa Y, Kanold PO, Majdan M, Shatz CJ. Multiple periods of functional ocular dominance plasticity in mouse visual cortex. *Nat Neurosci.* 2005;8:380–388.
16. John SW, Anderson MG, Smith RS. Mouse genetics: a tool to help unlock the mechanisms of glaucoma. *J Glaucoma.* 1999;8:400–412.
17. Anderson MG, Libby RT, Mao M, et al. Genetic context determines susceptibility to intraocular pressure elevation in a mouse pigmentary glaucoma. *BMC Biol.* 2006;4:20.
18. Senatorov V, Malyukova I, Fariss R, et al. Expression of mutated mouse myocilin induces open-angle glaucoma in transgenic mice. *J Neurosci.* 2006;26:11903–11914.
19. Keeler C. Retinal degeneration in the mouse is rodless retina. *J Hered.* 1966;57:47–50.
20. Bowes C, Li T, Danciger M, Baxter LC, Applebury ML, Farber DB. Retinal degeneration in the rd mouse is caused by a defect in the beta subunit of rod cGMP-phosphodiesterase. *Nature.* 1990;347:677–680.
21. Shearstone JR, Wang YE, Clement A, et al. Application of functional genomic technologies in a mouse model of retinal degeneration. *Genomics.* 2005;85:309–321.
22. Porciatti V, Pizzorusso T, Maffei L. The visual physiology of the wild type mouse determined with pattern VEPs. *Vision Res.* 1999;39:3071–3081.
23. Prusky GT, Reidel C, Douglas RM. Environmental enrichment from birth enhances visual acuity but not place learning in mice. *Behav Brain Res.* 2000;114:11–15.
24. Cook MN, Williams RW, Flaherty L. Anxiety-related behaviors in the elevated zero-maze are affected by genetic factors and retinal degeneration. *Behav Neurosci.* 2001;115:468–476.
25. Buhot MC, Dubayle D, Malleret G, Javerzat S, Segu L. Exploration, anxiety, and spatial memory in transgenic anophthalmic mice. *Behav Neurosci.* 2001;115:455–467.
26. Cancedda L, Putignano E, Sale A, Viegi A, Berardi N, Maffei L. Acceleration of visual system development by environmental enrichment. *J Neurosci.* 2004;24:4840–4848.
27. Schmucker C, Seeliger M, Humphries P, Biel M, Schaeffel F. Grating acuity at different luminances in wild-type mice and in mice lacking rod or cone function. *Invest Ophthalmol Vis Sci.* 2005;46:398–407.
28. Puk O, Dalke C, Favor J, de Angelis MH, Graw J. Variations of eye size parameters among different strains of mice. *Mamm Genome.* 2006;17:851–857.
29. Zhou G, Williams RW. Mouse models for the analysis of myopia: an analysis of variation in eye size of adult mice. *Optom Vis Sci.* 1999;76:408–418.
30. Schmucker C, Schaeffel F. In vivo biometry in the mouse eye with low coherence interferometry. *Vision Res.* 2004;44:2445–2456.
31. Schmucker C, Schaeffel F. A paraxial schematic eye model for the growing C57BL/6 mouse. *Vision Res.* 2004;44:1857–1867.
32. Zhou X, Shen M, Xie J, et al. The development of the refractive status and ocular growth in C57BL/6 mice. *Invest Ophthalmol Vis Sci.* 2008;49:5208–5214.
33. Chase HB. Studies on an anophthalmic strain of mice, III: results of crosses with other strains. *Genetics.* 1942;27:339–348.
34. Kalter H. Sporadic congenital malformations of newborn inbred mice. *Teratology.* 1968;1:193–199.

35. Koch FLP, Gowen JW. Spontaneous ophthalmic mutation in a laboratory mouse. *Arch Pathol Lab Med.* 1939;28:171–176.
36. Luan H, Roberts R, Sniegowski M, Goebel DJ, Berkowitz BA. Retinal thickness and subnormal retinal oxygenation response in experimental diabetic retinopathy. *Invest Ophthalmol Vis Sci.* 2006;47:320–328.
37. Schaeffel F, Burkhardt E, Howland HC, Williams RW. Measurement of refractive state and deprivation myopia in two strains of mice. *Optom Vis Sci.* 2004;81:99–110.
38. Avila MY, Carre DA, Stone RA, Civan MM. Reliable measurement of mouse intraocular pressure by a servo-null micropipette system. *Invest Ophthalmol Vis Sci.* 2001;42:1841–1846.
39. Straznicky C, Hiscock J. Post-metamorphic retinal growth in *Xenopus*. *Anat Embryol (Berl).* 1984;169:103–109.
40. Straznicky K, Gaze RM. The growth of the retina in *Xenopus laevis*: an autoradiographic study. *J Embryol Exp Morphol.* 1971; 26:67–79.
41. Rothstein H, Van Buskirk RG, Gordon SR, Worgul BV. Seasonal variations in mitosis in the frog: a field study. *Experientia.* 1975; 31:939–940.
42. Meyer RL. Evidence from thymidine labeling for continuing growth of retina and tectum in juvenile goldfish. *Exp Neurol.* 1978;59:99–111.
43. Raviola E, Wiesel TN. An animal model of myopia. *N Engl J Med.* 1985;312:1609–1615.
44. Smith EL 3rd, Bradley DV, Fernandes A, Boothe RG. Form deprivation myopia in adolescent monkeys. *Optom Vis Sci.* 1999;76: 428–432.
45. Troilo D, Nickla DL. The response to visual form deprivation differs with age in marmosets. *Invest Ophthalmol Vis Sci.* 2005; 46:1873–1881.
46. Gordon RA, Donzis PB. Refractive development of the human eye. *Arch Ophthalmol.* 1985;103:785–789.
47. Wallman J, Adams JI. Developmental aspects of experimental myopia in chicks: susceptibility, recovery and relation to emmetropization. *Vision Res.* 1987;27:1139–1163.
48. Prusky GT, Alam NM, Beekman S, Douglas RM. Rapid quantification of adult and developing mouse spatial vision using a virtual optomotor system. *Invest Ophthalmol Vis Sci.* 2004;45:4611–4616.
49. Norton TT, McBrien NA. Normal development of refractive state and ocular component dimensions in the tree shrew (*Tupaia belangeri*). *Vision Res.* 1992;32:833–842.
50. Qiao-Grider Y, Hung LF, Kee CS, Ramamirtham R, Smith EL 3rd. Normal ocular development in young rhesus monkeys (*Macaca mulatta*). *Vision Res.* 2007;47:1424–1444.
51. Fernandes A, Bradley DV, Tigges M, Tigges J, Herndon JG. Ocular measurements throughout the adult life span of rhesus monkeys. *Invest Ophthalmol Vis Sci.* 2003;44:2373–2380.
52. Larsen JS. The sagittal growth of the eye, IV: ultrasonic measurement of the axial length of the eye from birth to puberty. *Acta Ophthalmol (Copenh).* 1971;49:873–886.
53. Jones LA, Mitchell GL, Mutti DO, Hayes JR, Moeschberger ML, Zadnik K. Comparison of ocular component growth curves among refractive error groups in children. *Invest Ophthalmol Vis Sci.* 2005;46:2317–2327.
54. Zadnik K, Mutti DO, Mitchell GL, Jones LA, Burr D, Moeschberger ML. Normal eye growth in emmetropic schoolchildren. *Optom Vis Sci.* 2004;81:819–828.
55. Zadnik K, Manny RE, Yu JA, et al. Ocular component data in schoolchildren as a function of age and gender. *Optom Vis Sci.* 2003;80:226–236.
56. Shih YF, Chiang TH, Lin LL. Lens thickness changes among schoolchildren in Taiwan. *Invest Ophthalmol Vis Sci.* 2009;50:2637–2644.
57. Larsen JS. The sagittal growth of the eye, 1: ultrasonic measurement of the depth of the anterior chamber from birth to puberty. *Acta Ophthalmol (Copenh).* 1971;49:239–262.
58. Friedman NE, Mutti DO, Zadnik K. Corneal changes in schoolchildren. *Optom Vis Sci.* 1996;73:552–557.
59. Hasebe S, Ohtsuki H, Kono R, Nakahira Y. Biometric confirmation of the Hirschberg ratio in strabismic children. *Invest Ophthalmol Vis Sci.* 1998;39:2782–2785.
60. Baikoff G, Lutun E, Ferraz C, Wei J. Static and dynamic analysis of the anterior segment with optical coherence tomography. *J Cataract Refract Surg.* 2004;30:1843–1850.
61. Mutti DO, Mitchell GL, Jones LA, et al. Axial growth and changes in lenticular and corneal power during emmetropization in infants. *Invest Ophthalmol Vis Sci.* 2005;46:3074–3080.
62. Garner LF, Stewart AW, Owens H, Kinnear RF, Frith MJ. The Nepal Longitudinal Study: biometric characteristics of developing eyes. *Optom Vis Sci.* 2006;83:274–280.
63. Larsen JS. The sagittal growth of the eye, 3: ultrasonic measurement of the posterior segment (axial length of the vitreous) from birth to puberty. *Acta Ophthalmol (Copenh).* 1971;49:441–453.
64. Larsen JS. The sagittal growth of the eye, 2: ultrasonic measurement of the axial diameter of the lens and the anterior segment from birth to puberty. *Acta Ophthalmol (Copenh).* 1971;49:427–440.
65. Mutti DO, Zadnik K, Fusaro RE, Friedman NE, Sholtz RI, Adams AJ. Optical and structural development of the crystalline lens in childhood. *Invest Ophthalmol Vis Sci.* 1998;39:120–133.
66. Zadnik K, Mutti DO, Fusaro RE, Adams AJ. Longitudinal evidence of crystalline lens thinning in children. *Invest Ophthalmol Vis Sci.* 1995;36:1581–1587.
67. Glasser A, Campbell MC. Biometric, optical and physical changes in the isolated human crystalline lens with age in relation to presbyopia. *Vision Res.* 1999;39:1991–2015.
68. Schachar RA. Growth patterns of fresh human crystalline lenses measured by in vitro photographic biometry. *J Anat.* 2005;206: 575–580.
69. Atchison DA. Age-related paraxial schematic emmetropic eyes. *Ophthalmic Physiol Opt.* 2009;29:58–64.
70. Atchison DA, Markwell EL, Kasthurirangan S, Pope JM, Smith G, Swann PG. Age-related changes in optical and biometric characteristics of emmetropic eyes. *J Vis.* 2008;8:29:1–20.
71. Qiao-Grider Y, Hung LF, Kee CS, Ramamirtham R, Smith EL 3rd. A comparison of refractive development between two subspecies of infant rhesus monkeys (*Macaca mulatta*). *Vision Res*. 2007;47: 1668–1681.
72. Augusteyn RC. Growth of the human eye lens. *Mol Vis.* 2007;13: 252–257.
73. Chalupa LM, Williams RW. *Eye, Retina, and Visual System of the Mouse.* Cambridge, MA: MIT Press; 2008:xii, 754.
74. Woolf D. A comparative cytological study of the ciliary muscle. *Anat Rec.* 1956;124:145–163.
75. Barathi VA, Boopathi VG, Yap EP, Beuerman RW. Two models of experimental myopia in the mouse. *Vision Res.* 2008;48:904–916.
76. Pardue MT, Faulkner AE, Fernandes A, et al. High susceptibility to experimental myopia in a mouse model with a retinal on pathway defect. *Invest Ophthalmol Vis Sci.* 2008;49:706–712.
77. Glickstein M, Millodot M. Retinoscopy and eye size. *Science.* 1970; 168:605–606.
78. Preece SJ, Claridge E. Monte Carlo modelling of the spectral reflectance of the human eye. *Phys Med Biol.* 2002;47:2863–2877.
79. Hammer M, Roggan A, Schweitzer D, Muller G. Optical properties of ocular fundus tissues—an in vitro study using the double-integrating-sphere technique and inverse Monte Carlo simulation. *Phys Med Biol.* 1995;40:963–978.
80. Delori FC, Pflibsen KP. Spectral reflectance of the human ocular fundus. *Appl Opt.* 1989;28:1061–1077.
81. Gorrand JM. Separation of the reflection by the inner limiting membrane. *Ophthalmic Physiol Opt.* 1986;6:187–196.
82. Knighton RW, Baverez C, Bhattacharya A. The directional reflectance of the retinal nerve fiber layer of the toad. *Invest Ophthalmol Vis Sci.* 1992;33:2603–2611.
83. Knighton RW, Jacobson SG, Kemp CM. The spectral reflectance of the nerve fiber layer of the macaque retina. *Invest Ophthalmol Vis Sci.* 1989;30:2392–2402.